Materials Horizons

ROYAL SOCIETY OF CHEMISTRY

COMMUNICATION

View Article Online
View Journal

Cite this: DOI: 10.1039/d6mh00641h

Design of polymer-based CO_2-membrane adsorbers for carbon capture

Emil Pashayev and Prokopios Georgopanos *

Received 1st April 2026,
Accepted 5th June 2026

DOI: 10.1039/d6mh00641h

rsc.li/materials-horizons

This study focuses on the CO_2 capture performance of poly(*N*,*N*-dimethylaminopropyl acrylamide) (PDMAPAm) and poly(*N*-[3-(dimethylamino)propyl]-acrylamide)-*b*-poly(methyl methacrylate) (PDMAPAm-*b*-PMMA) diblock copolymers for fabrication of CO_2-responsive membrane adsorbers. By systematically varying the block composition of the diblock copolymer PDMAPAm-*b*-PMMA, optimal compositions for maximizing CO_2 adsorption capacity are identified. The adsorption mechanisms were characterized under both dry and humid conditions, revealing distinct physisorption and chemisorption pathways. The first major novelty of this work is the creation of a unified kinetic model that, for the first time, integrates polymerization kinetics with adsorption kinetics, allowing the CO_2 uptake capacity of membrane adsorbers to be directly predicted from the underlying polymer properties. A second key innovation is the use of this unified model to rationally design and fabricate a polymer membrane adsorber that achieves a CO_2 uptake capacity of 6 mmol g^{-1}, substantially exceeding the performance of commercially available polymer-based sorbents.

New concepts

In this paper, we present the design and development of novel CO_2-responsive polymer membrane adsorbers, encompassing both homopolymers, poly(*N*,*N*-dimethylaminopropyl acrylamide) (PDMAPAm) and diblock copolymers, poly(*N*-[3-(dimethylamino)propyl]acrylamide)-*b*-poly(methyl methacrylate) (PDMAPAm-*b*-PMMA). These advanced materials exhibit a markedly higher CO_2 uptake capacity (approximately 6 mmol g^{-1}) compared to conventional polymer-based membrane adsorbers reported in the literature, such as polyethyleneimine (PEI), tetraethylenepentamine (TEPA), polyacrylonitrile (PAN), polypropylenimine (PPI), and their composites. This is a new concept in the field of polymers for storage of CO_2. A detailed investigation of adsorption mechanisms reveals distinct physisorption and chemisorption pathways, highlighting the critical steps that govern CO_2 capture performance in these newly developed polymers. Furthermore, the methodology underlying the creation of these membrane adsorbers is unique: it integrates experimental synthesis with digital modeling through a unified framework that couples polymerization reaction kinetics with CO_2 adsorption kinetics—a combined approach that, to our knowledge, has not been previously reported. This synergy between material design and process modeling establishes a new paradigm for engineering high-performance CO_2 adsorbents.

Introduction

One of the most critical aspects of our days is reducing our carbon footprint to avoid further negative impacts on the climate. Along with traditional methodologies for reducing CO_2 emissions, such as membrane separation technologies, another technology, direct air capture (DAC), has recently come into focus. DAC represents a cutting-edge approach for mitigating climate change by selectively removing carbon dioxide (CO_2) from ambient air, offering a scalable solution to reduce atmospheric greenhouse gas concentrations.[1–6] This process utilizes adsorbent materials that selectively capture and retain CO_2 molecules from atmospheric air.[2,7,8] In a typical DAC system, ambient air is directed through a contactor where it flows over the surface of the adsorbent material.[6,9] CO_2 molecules are adsorbed onto the material surface *via* physical interactions (physisorption) or chemical bonding (chemisorption).[6,9,10]

Gas adsorption on solid surfaces generally occurs *via* two primary mechanisms: physisorption and chemisorption. Physisorption (or physical adsorption) arises from weak intermolecular forces, such as van der Waals interactions, leading to a more reversible and less specific attachment of gas molecules to the surface.[11,12] In contrast, chemisorption, also known as chemical adsorption, involves the formation of chemical bonds between gas molecules and the surface of the adsorbent, resulting in a stronger and often more specific interaction.[13,14] Chemical adsorption, also known as irreversible adsorption, involves a substantial electron exchange between the adsorbate molecules and the adsorbent's surface. This process results in the formation of covalent or ionic bonds[15] and is characterized by strong interaction potentials, leading to high adsorption temperatures that often approach those of chemical bonds (80–240 kJ mol^{-1}).[16]

Helmholtz-Zentrum Hereon, Institute of Membrane Research, Max-Planck-Str. 1, 21502 Geesthacht, Germany. E-mail: prokopios.georgopanos@hereon.de

As with most chemical reactions, it typically requires a specific activation energy to return the system to an equilibrium state. The physisorption occurring between dry CO_2 and polymer has been investigated in our last publication.[17] Therefore, the present study primarily investigates chemisorption phenomena alongside physisorption.

The advancement and optimization of adsorbent materials are pivotal for enhancing the efficiency and scalability of DAC technologies.[2,18] Diblock copolymers have demonstrated strong potential for CO_2 capture, mainly due to the high affinity between amine groups and CO_2 molecules.[19,20] In particular, diblock copolymers incorporating amine-functional segments such as poly(2-(dimethylamino)ethyl methacrylate) (PDMAEMA),[21–24] poly(*N*,*N*-dimethylallylamine) (PDMAAm),[25–28] poly(2-aminoethyl methacrylate) (PAEM),[29,30] and poly(*N*,*N*-dimethylaminopropyl acrylamide) (PDMAPAm)[31] have emerged as promising candidates for DAC applications. These materials exhibit high CO_2 reactivity and selectivity,[21,31,32] high porosity,[33–37] and scalability for industrial deployment.[31,38–40]

In this study, the used PDMAPAm-based block copolymers were developed *via* RAFT polymerization rather than conventional free-radical polymerization, as RAFT is a controlled radical polymerization technique that provides precise control over molecular weight, dispersity, and polymer composition, enabling the straightforward preparation of well-defined block copolymers.[40–42] Block copolymer architecture was selected to precisely tune the microenvironment around the CO_2 responsive amines and to control film mechanical stability, morphology, segmental mobility, and hydrophilicity factors that strongly influence adsorption behavior, especially under humid conditions.[17] As mentioned in the previous publication,[17,40,41] for synthesizing the PDMAPAm-*b*-PMMA diblock copolymer, the lengths of the two blocks were deliberately chosen to achieve a balance between a high proportion of CO_2-responsive tertiary amines for effective sorption and a sufficiently long PMMA segment to provide the mechanical robustness required for membrane fabrication. This level of structural control is not achievable with free radical homopolymers.

As demonstrated in our previous publication,[17,40,41] an integrated computational and experimental unified model was developed to design acrylamide-based polymers with tailored CO_2 affinity and transport characteristics. Within this context, CO_2-responsive polymers such as PDMAPAm and PDMAPAm-*b*-PMMA were synthesized and their CO_2 uptake under dry conditions was experimentally quantified, allowing the measured uptake to be linked to the underlying solution–diffusion and adsorption mechanisms.[2,4] In parallel, our earlier work established a comprehensive understanding of CO_2 transport in PDMAPAm- and PDMAPAm-*b*-PMMA-coated membranes used as selective layers, showing that these materials can achieve CO_2/N_2 permeability selectivities of up to 10–15, indicative of their strong CO_2-responsive behavior.[40,41] SEM analyses confirmed that the selective layers form dense, continuous, and nonporous structures in which gas transport is governed by polymer–gas interactions rather than convective flow, consistent with the solution–diffusion mechanism in which gas molecules dissolve into the polymer matrix and subsequently diffuse through it.[40,43] Together, these findings highlight that these polymers exhibit both high CO_2 uptake and well-defined transport behaviour, providing a natural foundation for the development of membrane adsorbers that integrate dense-layer permeation with sorbent-like adsorption functionality.

A membrane adsorber is a flat sheet thin-film that combines the dense selective layer of a membrane with the functional adsorption sites of a sorbent, creating a material capable of both solution–diffusion-based permeation[40,41] and affinity-driven adsorption.[17] This dual mechanism allows gases or solutes to dissolve and diffuse through the polymer matrix while simultaneously interacting with embedded adsorption sites, resulting in enhanced selectivity, higher uptake capacity, and faster mass-transfer performance compared to conventional membranes or sorbents alone.

This study primarily investigates the humid CO_2 sorption behavior of the CO_2-responsive PDMAPAm-based CO_2-responsive membrane adsorbers, with particular emphasis on their sorption kinetics. In addition to quantifying the contributions of physisorption and chemisorption under humid conditions that more closely resemble realistic atmospheric environments, the work clarifies how these sorption processes couple with the polymerization kinetics of the materials such as PDMAPAm and PDMAPAm-*b*-PMMA.[40,42] By integrating sorption kinetics and polymerization kinetics into a unified model, the study provides a unified model framework that links polymer structure formation to CO_2 uptake performance. Through systematic variation of temperature, pressure, and relative humidity of CO_2 capture conditions, polymer properties the CO_2 capture capacity of the materials is optimized, revealing how both material design and process conditions govern overall performance.

Experimental

Material and methods

The reagents and materials employed in the synthesis of the polymers in this study were the same as those previously described in our earlier publication,[17] ensuring consistency in the experimental conditions and comparability of results.

Synthesis of PDMAPAm and PDMAPAm-*b*-PMMA

PDMAPAm and PDMAPAm-*b*-PMMA diblock copolymer used in this study were synthesized *via* RAFT polymerization following the procedure reported in our previous work.[17] Detailed procedure and recipe of the synthesis were given in the SI.

The synthesis protocol of $PMMA_{70}$ can be found in our previous publication[38] and polymer properties is described in the Table S4 in the SI.[17]

Characterization

Gel permeation chromatography (GPC)

The molecular weight profiles of PDMAPAm homopolymers and PDMAPAm-*b*-PMMA diblock copolymers were determined

using gel permeation chromatography (GPC) as shown in our previous work.[17] Detailed information regarding the polymer characterization in the GPC was given in the SI.

Proton nuclear magnetic resonance (NMR)

^{1}H NMR spectroscopy experiments were conducted following the procedure described in a previous publication.[17] A detailed description of the measurement protocol is provided in the SI.

DMAPAm conversion from macro-RAFT synthesis was estimated by comparing the integration of double-bond proton areas in the sample before and after the reaction, which was around 90%. Using the same method,[40] the conversion of methyl methacrylate in the second block synthesis, also measured in CDCl3, was calculated from the decrease in the integral of the monomer peaks, which was also approximately 90%.

InfraSORP device by Fraunhofer IWS

The INFRAsorp device developed by Fraunhofer IWS (Dresden, Germany) is an optical calorimeter that quantifies adsorption-induced heat release to characterize porous materials. During measurement, a test gas flows over the sample, initiating adsorption on its surface. The heat released from adsorption causes a temperature increase, which is detected by an infrared sensor positioned above the sample. The resulting thermal signal appears as a peak, and its area is directly proportional to the total heat of adsorption, reflecting the amount of gas adsorbed.[44–46] By knowing the specific heat capacity of the polymer (PDMAPAm) from the DSC measurement[40] and the integrated area under the temperature peak, the heat release arising from the gas adsorption can be estimated.

Open quartz crystal microbalance (openQCM Q^{-1})

Adsorption measurement (chemisorption) of wet CO_2 has been conducted using the openQCM Q^{-1} device (Novaetech Srl, Pompeii, Italy). The openQCM Q^{-1} M is a Quartz Crystal Microbalance device that can simultaneously measure both frequency and dissipation changes of the quartz crystal at the same time. This allows for assessing variations in mass and the viscoelastic properties of the material on the quartz crystal's surface. The core sensing element of the QCM is a thin AT-cut quartz crystal equipped with electrodes on both sides. Prior to measurement, the crystal surface was uniformly coated with a PDMAPAm-based polymer film ($\approx$130 μm thickness) by drop-casting a THF solution, followed by controlled solvent evaporation. During the measurements, the coated crystal was placed inside the QCM chamber and exposed to a continuous gas flow (CO_2 or N_2). For humid-gas experiments, the gas stream was bubbled through deionized water for 1 h, and the resulting relative humidity was monitored in real time using an inline humidity sensor. The flow rate, temperature, and pressure inside the chamber were kept constant throughout each experiment.

When the coated crystal is exposed to a gas stream, the polymer film interacts with the incoming gas molecules. Adsorption of gas onto the polymer increases the mass of the film, which in turn causes a measurable decrease in the resonant oscillation frequency of the quartz crystal. This frequency shift is detected through the electrodes.

The magnitude of the frequency change is directly proportional to the mass change on the crystal surface. This relationship is described by the Sauerbrey equation[48] shown below:

$$\frac{\Delta F}{n} = \frac{-2f_0^2}{A\sqrt{\rho_q \mu_q}}\Delta m$$

f_0 is the resonant frequency of the crystal (10 MHz), Δm is the mass change, A is the piezoelectrically active crystal area (0.320 cm^2), ρ_q is the density of quartz (2.648 g cm^{-3}), and μ_q is the shear modulus of an AT-cut crystal (2.947×10^{11} g cm^{-1} s^{-2}).

By tracking the real-time frequency changes, a quartz crystal microbalance (openQCM Q^{-1}) can provide valuable insights into the amount of mass deposited and the rate at which these films are added or removed.[47,48]

Fourier transform infrared spectroscopy (FTIR)

To investigate changes in functional groups following chemisorption, a film of PDMAPAm (thickness = 10 μm) coated onto the quartz crystal of openQCM Q^{-1} device was examined using Fourier Transform Infrared (FTIR) spectroscopy. Spectra were recorded before and after exposing the film to dry N_2, humid N_2, and humid CO_2. However, this measurement was not carried out with dry CO_2, because in the absence of water, it does not chemically react with tertiary amines to form covalent bonds[49,50] that could be detected as characteristic peaks in the FTIR spectrum. The measurements were performed using a Bruker ALPHA FTIR spectrometer (Bruker, Ettlingen, Germany) in attenuated total reflectance (ATR) mode. Data were collected at room temperature over a spectral range of 600–4000 cm^{-1}, with a resolution of 4 cm^{-1} and averaged over 64 scans.

Results and discussion

The synthesized polymers, PDMAPAm and its diblock copolymer, PDMAPAm-*b*-PMMA, were systematically characterized to evaluate their chemical and physical interactions with CO_2 under both dry and humid conditions. Comparative analyses were conducted using PDMAPAm homopolymers and PDMAPAm-*b*-PMMA copolymers featuring a constant PDMAPAm block and varying PMMA block lengths and measurements were conducted at different temperatures to follow Arrhenius parameters of reaction coefficients.

Mechanism of dry and humid CO_2 adsorption

As illustrated in Fig. 1, the diblock copolymer PDMAPAm-*b*-PMMA consists of two distinct polymer blocks: poly(*N*,*N*-dimethylaminopropylacrylamide) (PDMAPAm) and poly(methyl methacrylate) (PMMA). The PDMAPAm segment contains functional groups such as amides (comprising carbonyl and secondary amine functionalities) and tertiary amines. Upon exposure to dry CO_2, these functional groups are theoretically capable of interacting with CO_2 molecules, suggesting a potential for selective and efficient adsorption *via* chemical affinity.[51,52] The

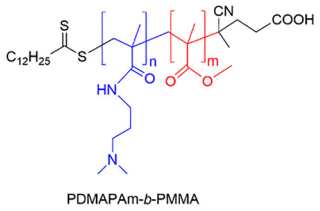

PDMAPAm-*b*-PMMA

Fig. 1 Chemical structure of the diblock copolymer PDMAPAm-*b*-PMMA synthesized *via* RAFT polymerization.

interaction of both PDMAPAm and PMMA blocks within the diblock copolymer with dry CO_2 has been discussed in greater detail in our previous publication.[17] Given that the concentration of RAFT end groups is significantly lower than that of the functional groups present on the monomeric units, their interaction with dry or humid CO_2 can be considered negligible.

In humid conditions, the amides on PDMAPAm block are relatively stable compounds due to resonance between the nitrogen lone pair and the carbonyl group. This makes them less reactive with humid CO_2 than amines.[53–56] Tertiary amines chemically interact with humid CO_2 *via* the following pathway shown in Fig. 2.

This mechanism, which involves the base-catalyzed hydration of CO_2, was initially documented by Donaldson[57] and later examined by Kenig[58] and involves a two-step reaction sequence. Initially, the tertiary amine reacts with water vapor to produce an ammonium ion and a hydroxide ion. The hydroxide ion subsequently reacts with CO_2 to form a bicarbonate ion. Finally, the resulting bicarbonate and ammonium ions associate to form a stable bicarbonate salt. In this scenario, CO_2 does not chemically react with tertiary amines in the absence of water (*i.e.*, under dry conditions). For the chemical interaction between CO_2 and tertiary amine, the existence of water vapor is crucial.[49,50]

Since the CO_2 uptake of PMMA homopolymer under dry conditions does not significantly differ from its uptake under humid conditions, the contribution of the PMMA block to the overall CO_2 adsorption capacity of the diblock copolymer in humid environments is considered negligible (see SI).

Validation of adsorption results from openQCM Q^{-1}

To start with, several adsorption measurements have been conducted to analyze the dry CO_2 capture performance of the synthesized CO_2-responsive polymer, PDMAPAm, in the two different devices, in a gravimetric adsorption device and in an openQCM Q^{-1} for comparison of both results. The results of the comparison are represented in Fig. 3. It is crucial to note that the PDMAPAm sample was measured as film (30% w/w polymer in THF), both in the gravimetric adsorption device and openQCM Q^{-1}.

Fig. 3 presents a comparison of the dry CO_2 uptake capacities of PDMAPAm measured in film form using two different analytical devices: the open QCM Q^{-1}, which measures changes in resonance frequency corresponding to mass variation during CO_2 adsorption, and the gravimetric adsorption system, with data published elsewhere.[17] As shown in Fig. 3, the CO_2 uptake values obtained between 0.6 and 1.5 bar are nearly identical across both measurement techniques. This consistency indicates that the adsorption results from the open QCM Q^{-1} are in good agreement with those obtained from the gravimetric adsorption device. Therefore, in this study, an open QCM Q^{-1} device was utilized to measure the adsorption capacity of polymers as a film in both dry and wet conditions.

Humid CO_2 adsorption–desorption

Furthermore, at atmospheric pressure, CO_2 uptake capacities of homopolymer ($PDMAPAm_{232}$) and diblock copolymer ($PDMAPAm_{232}$-*b*-$PMMA_{57}$) were measured in dry and humid conditions by building the following system (Fig. 4). For humid CO_2 (or similarly for humid N_2) measurements, the gas is bubbled into a closed Schott–Duran bottle, which is partially filled with water (20 mL of 1000 mL) for 1 hour at room temperature. Meanwhile, pressure and relative humidity of the wet gas going to the QCM Q^{-1} device were measured using the manometer and the relative humidity measurement device connected to the bottle. The main part of the QCM Q^{-1} device is the cell where the quartz crystal is located. The crystal is coated with polymer (10% w/w dissolved in THF). The thickness of the coating is around 130 micrometers. In the cell, a temperature sensor provides the temperature of the wet gas whereas the electrodes of the quartz crystal provide information regarding the resonance frequency change related to mass change as wet CO_2 is being adsorbed. For the dry gas measurement, the same measurement is conducted without water in the bottle.

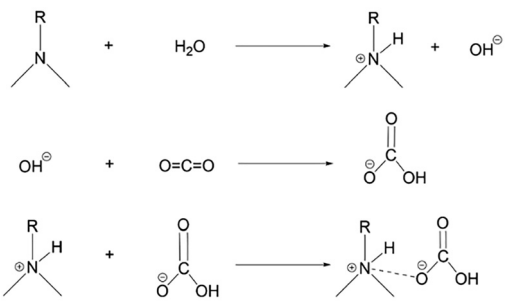

Fig. 2 Chemical interaction mechanism of tertiary amine with humid CO_2.

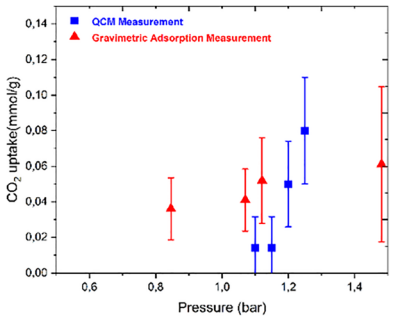

Fig. 3 Comparison of CO_2 uptake of PDMAPAm as film measured in openQCM Q^{-1} with CO_2 uptake measured with the gravimetric adsorption device.

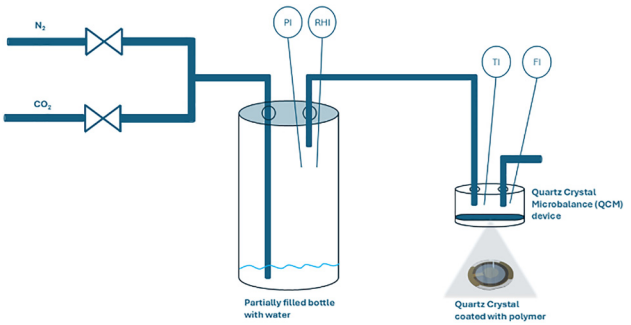

Fig. 4 Sorption measurement using openQCM Q^{-1} device. PI – Pressure indicator, RHI – relative humidity indicator, TI – temperature indicator, FI – frequency indicator.

Sorption measurements on the QCM Q^{-1} device were conducted with dry and wet CO_2 and wet N_2, and the results are presented in Fig. 5.

Fig. 5 represents the evolution of CO_2 and N_2 uptake by $PDMAPAm_{232}$ in dry and humid conditions (RH = 55%). This is clear from the figure that generally, in dry conditions, a small amount of CO_2 was captured by the $PDMAPAm_{232}$, which is almost the same amount as captured in another adsorption device mentioned before. In contrast, at RH = 55%, the $PDMAPAm_{232}$ shows quite a higher uptake for humid CO_2 and N_2 gases. As many other amine-based polymer sorbents exhibit higher CO_2 capacity in humid conditions than in dry conditions,[59,60] the $PDMAPAm_{232}$ shows the same trend. In other words, 8–9 times more CO_2 was captured in humid conditions than in dry conditions, and the difference in CO_2 capture amount between humid and dry conditions is around 2–4 times in other publications.[60–62] Another consideration is that the Fig. 5 shows that the weight of polymer is increased in the humid CO_2-exposure case more than in the humid N_2-exposure case under the same temperature, pressure and humidity conditions (55%). If dry CO_2 uptake and humid N_2 uptake are subtracted from humid CO_2 uptake of the polymer, the difference is obtained to be around 0.01 g g^{-1}. This difference increases up to 0.07 g g^{-1} as the humidity turns to be 75% as shown in Table 1.

There can be two reasons for the observed variation. First reason can be that monomeric units of $PDMAPAm_{232}$ have a

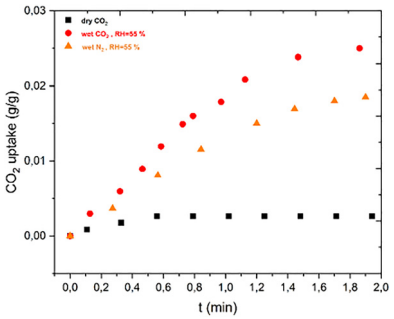

Fig. 5 CO_2 and N_2 uptake of homopolymer $PDMAPAm_{232}$ in dry and humid conditions.

Table 1 CO_2 and N_2 uptake of homopolymer $PDMAPAm_{232}$ in dry and humid conditions (RH = 75%)

Conditions	Uptake (g g^{-1})
Dry CO_2	4.000×10^{-3}
Humid CO_2	1.080×10^{-1}
Humid N_2	3.747×10^{-2}

tertiary amine on them that can chemically react with humid CO_2 and it can be chemisorbed onto the polymer, which can lead to the formation of ammonium bicarbonate.[57,58] The second reason could be that in dry environments, tertiary amines with bulky substituents (like two methyl groups) exhibit limited accessibility for CO_2 due to steric hindrance.[63–66] In the presence of water and CO_2, tertiary amines can become protonated[57,58] and this protonation may reduce steric hindrance, polarity and hydrogen bonding capacity of the nitrogen site, potentially opening up access for CO_2 molecules to interact *via* physical adsorption.[67] The protonation enhances hydration shells and facilitates CO_2 mass transfer.[68] However, if the homopolymer $PMMA_{70}$ is exposed to CO_2 in dry and humid conditions, there is no change in the CO_2 uptake of PMMA in humid conditions compared to in dry conditions (see Table S5 in SI). This is because there is no functional group that can be protonated, unlike in PDMAPAm.

To investigate where the difference exactly arises, additionally, before and after each openQCM Q^{-1} measurement of the polymer films, they are washed with nitrogen gas for one day at atmospheric pressure and room temperature, and the polymer film mass is measured in a weight balance to see how the mass of polymer after the capturing process was changed. The results of the mass change of $PDMAPAm_{232}$ are illustrated in Table 2.

The theory behind is that if the polymer is washed with N_2 after each measurement, physically adsorbed gas molecules has to desorb easier than chemically adsorbed gas molecules because physisorption is a reversible process involving weak van der Waals interactions and the energy released during adsorption is comparable to the energy required for desorption[69,70] whereas in chemisorption case, desorption requires significantly more energy than physisorption due to the formed strong chemical bonds.[71,72] This can be clearly seen from the Table 2, which compared to the humid N_2 and dry CO_2 cases, the highest weight change, which is stable regardless of N_2 washing after exposure, occurs when the polymer film interacts with humid CO_2, which is around 1.175×10^{-2} g g^{-1} at RH = 75%. It means that more energy is required to desorb all the adsorbed gas molecules from the polymer. So, the reason for the remaining gas molecules inside the polymer can be chemically adsorbed CO_2 gas

Table 2 Captured weight by polymer $PDMAPAm_{232}$ exposing to dry CO_2 and humid CO_2 (RH = 75%) and N_2

Conditions	Captured weight (g g^{-1})
After dry CO_2-exposure and N_2 washing	1.008×10^{-4}
After humid CO_2-exposure and N_2 washing	1.175×10^{-2}
After humid N_2-exposure and N_2 washing	5.002×10^{-4}

molecules that reacted with the tertiary amines of the polymer, leading to the formation of ammonium bicarbonate.[57,58] Considering that the polymer PDMAPAm (36 kDa) has approximately 230 monomeric units (in each monomeric unit, one tertiary amine) and a 1 : 1 reaction would occur between the tertiary amine and humid CO_2, theoretically, uptake of the polymer film *via* chemisorption had to be 0.280 g g^{-1}. This can mean that only some (about 7%) of the tertiary amines have reacted. As shown in our previous publication,[40,41] the film, which was fabricated, is thick and dense. The research group of J. R. Hoffman *et al.*[73,74] has reported that, in the thick-film regime, CO_2 capture is primarily limited by the accessibility of amine sites, and amine groups located deeper within the film are often inaccessible and therefore do not effectively participate in the reaction. In other words, when the polymer thickness is higher, interaction between CO_2 and the amine group occurs only on the surface. Hence, only a few percent of tertiary amines have reacted.

Table 2 shows that the chemisorbed CO_2 uptake of the polymer under humid conditions (RH = 75%) is approximately 1.175×10^{-2} g g^{-1} whereas Table 1 indicates that the difference in total uptake between samples exposed to humid CO_2 and humid N_2 at the same humidity level is about 0.07 g g^{-1}, which is five to six times greater than the chemisorbed CO_2 fraction. Overall, when the polymer is exposed to humid CO_2 at 75% RH, the total CO_2 uptake is 0.07 g g^{-1}, of which 1.175×10^{-2} g g^{-1} corresponds to chemisorption and 0.058 g g^{-1} to physisorption. This clearly demonstrates that, under humid conditions, the dominant CO_2 capture mechanism in the polymer is physical adsorption rather than chemical adsorption.

Another noteworthy observation is that, under humid conditions, the amount of CO_2 physically adsorbed by the polymer (0.058 g g^{-1}) is an order of magnitude greater than its CO_2 uptake capacity under dry conditions. This means that in the presence of water and CO_2, tertiary amines can become protonated[57,58] and this protonation may reduce the steric hindrance mentioned before and it increases the polarity and hydrogen bonding capacity of the nitrogen site, which potentially opens up access for CO_2 molecules to interact *via* physical adsorption[67] and facilitates CO_2 mass transfer.[68] As a result, more CO_2 molecules are physically adsorbed.

To sum it all up, when the polymer is exposed to humid CO_2, the total adsorbed gas consists of physically adsorbed CO_2 and water vapor molecules, as well as chemically adsorbed CO_2 molecules.

Moreover, the openQCM Q^{-1} quartz crystal can also measure dissipation values within the experiment. Dissipation (ΔD) reveals details about the viscoelastic nature of the adsorbed layer. A higher ΔD value suggests the layer is more viscoelastic—such as being soft, hydrated, or swollen—while a lower ΔD indicates a more rigid and less flexible film. Dissipation value changes of the adsorbed layer (which is polymer film) before and after exposures to dry CO_2, humid CO_2 and humid N_2 are observed and the increase percentage (%) of dissipation values were determined. At the same time, using the device, called Infrasorp, which is an optical calorimeter, the heat release from the polymer during adsorption of dry CO_2, humid CO_2 and humid N_2 was measured.

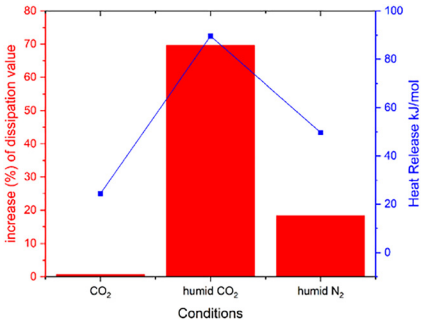

Fig. 6 Dissipation value change and heat release of adsorbed layer with exposure to dry CO_2, humid CO_2 and humid N_2.

Fig. 6 shows the increased percentage (%) of dissipation values and heat release after the polymer, $PDMAPAm_{232}$, is exposed to dry CO_2, humid CO_2 and humid N_2.

It can be clear from the figure that the highest dissipation value change and highest heat release is observed when the polymer layer is exposed to humid CO_2 and the figures are relatively lower in humid N_2-exposure case which is followed by dry CO_2-exposure case.

Upon exposure to humid CO_2, the polymer film exhibits pronounced interactions, likely due to the synergistic effects of CO_2 and water vapor. These interactions may involve the formation of bicarbonate ions or enhanced polymer hydration, resulting in significant softening or swelling of the material. This hypothesis is supported by the observed heat release of approximately 90 kJ mol^{-1}, which closely aligns with literature values[16,20,68,75,76] for the exothermic reaction that can potentially occur between tertiary amines and humid CO_2 leading to bicarbonate ion formation.

In contrast, exposure to humid N_2 results in a comparatively lower change in dissipation, likely attributable to water uptake alone. This can induce moderate swelling or plasticization of the polymer. The associated heat release, which is approximately 50 kJ mol^{-1}, during humid N_2 adsorption is consistent with values[68] typical of physisorption, likely driven by hydrogen bonding interactions. These findings indicate that humid N_2 is adsorbed onto $PDMAPAm_{232}$ primarily through physisorption mechanisms.

Simulation of humid CO_2 adsorption

Several kinetic models have been reported in the literature, including the Pseudo-First-Order (PFO),[77] Pseudo-Second-Order (PSO),[77–80] Elovich,[143] and Avrami[81] models. Out of the models, only PSO and Avrami models were selected for fitting. The reason for this is that studies show PSO provides the best fit for CO_2 adsorption on amine-functionalized materials across various temperatures and concentrations[77,82] and also Avrami model can describe the system that involve both chemisorption and physisorption.[81]

The PSO model correlates the amount adsorbed with the square of the available sites.[78] It assumes that the interactions between the adsorbent and adsorbate arise from the strong binding of adsorbate molecules to the adsorbent's surface,

making this model suitable for chemisorption-based CO_2 adsorption.[78–80] The model is represented as follows:

$$q_t = \frac{q_e^2 k_2 t}{1 + q_e k_2 t}$$

The Avrami model describes Fractional-order kinetics and multi-step adsorption considering complexity of dual chemisorption/physisorption.[80,81] This model is described by the following equation:

$$q_t = q_e\left(1 - e^{-k_A t^{n_A}}\right)$$

In these equations, q_t and q_e represent the adsorption capacity (mmol CO_2 per g) at time t (minutes) and at equilibrium, respectively. The constants k_2 and k_A correspond to the PSO and Avrami rate constants, respectively. The Avrami exponent (n_A) indicates the changes in the mechanism occurring during the adsorption process.[80]

The impact of relative humidity on the kinetic studies of CO_2 adsorption onto $PDMAPAm_{232}$ was investigated at 25 °C using four different relative humidity levels (0%, 55%, 65%, 75 and 85%). Both kinetic models – Avrami and PSO models—were applied to analyze the experimental data. Using the two different models, the fitting has been done and the results of fitting are depicted in the Fig. 7 and Table 3.

The Fig. 7 represents fitting of experimental CO_2 uptake data collected to two different adsorption models. It can be clearly seen from the graphs that both Avrami and PSO models predict adsorption of humid CO_2 precise. Compared to the PSO, the Avrami model for low humidity cases (such as RH = 55 and 65%) has relatively more accurate prediction. The Avrami model captures surface restructuring, nucleation, and growth of adsorbed layers, which are more pronounced under low humidity due to reduced water-mediated mobility of CO_2 and slower diffusion, making surface phenomena more dominant. Apart from that, under humid conditions, CO_2 undergoes both physical and chemical adsorption. As previously noted, at lower humidity levels, the extent of chemisorption decreases, resulting in a relatively higher contribution from physisorption. Given that the Avrami model accounts for both chemisorption and physisorption processes, unlike the pseudo-second-order model which primarily describes chemisorption, this may explain why the Avrami model tends to provide a better fit under conditions of lower humidity.

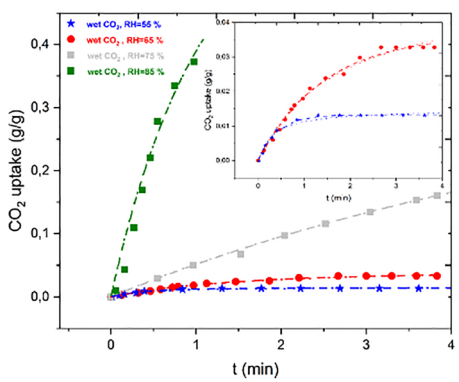

Fig. 7 Fitting of two different models for description of adsorption of humid CO_2. Dashed lines (—) show Avrami model. Dot lines (. . .) show PSO model.

Table 3 *R*-Square (R^2) values from fitting with the first and PSO model

Experiment	*R*-Square (avrami model)	*R*-Square (PSO model)
Dry CO_2	0.98700	0.95416
Wet CO_2, RH = 55%	0.99885	0.99879
Wet CO_2, RH = 65%	0.99522	0.97413
Wet CO_2, RH = 75%	0.99996	0.98533
Wet CO_2, RH = 85%	0.99995	0.95401

The Table 3 describes *R*-square (R^2) values from fitting of experimental values with the Avrami model and PSO model. *R*-Square tells how much of the variation in the experimental data is captured by the model. It can be clearly seen from the Table 3, compared to R^2 values of PSO model, the values of the Avrami model are closer to 1. This also means that the Avrami model predicts adsorption in humid conditions better than the PSO model does. Considering the better fitting results, the Avrami model is chosen for the description of the adsorption of humid CO_2 onto the polymer.

The fitting of the Avrami model has been done for various humid CO_2 adsorption experiments and the kinetic parameters of the Avrami model at all these different relative humidities have been recorded. The calculated kinetic parameters of the Avrami model for humid CO_2 capture with variation of relative humidity is shown in the Fig. 8.

This is clear from Fig. 8 that q_e increases and k_A values decrease as relative humidity increases. Another critical point is that a big increase is observed for the q_e – values as the relative humidity changes from 65% to 75%. This kind of sudden increase in q_e value is observed for PEI film described in another publication.[73] This might be related to the fact that starting from RH = 75%, more chemisorption occurs between the tertiary amine group on each monomeric unit, leading to a huge mass rise, which increases the q_e value significantly in the end.

In summary, the adsorption of dry CO_2 onto the PDMAPAm polymer follows the Langmuir model,[17] while adsorption in humid conditions is better described by the Avrami model. In both cases, the rate constants play a critical role, as they help assess the minimum energy barrier required for CO_2

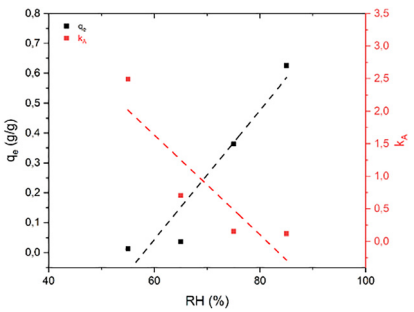

Fig. 8 Change of Avrami model kinetic parameters with relative humidity.

adsorption under these distinct conditions. This energy barrier is quantified by the activation energy (E_a), which can be determined through the linearization of the Arrhenius equation described below and the result is demonstrated in Fig. 9.

$$\ln(k) = -\frac{E_a}{RT} + \ln(A)$$

where k is a rate constant, for Langmuir model is k_L and for Avrami model is k_A. E_a is the activation energy, R is the universal gas constant, A is an Arhenius pre-exponential factor and T is the absolute temperature.[83]

Fig. 9 illustrates the natural logarithm of the rate constant ($\ln(k)$) as a function of the inverse of the adsorption temperature $\left(\frac{1}{T}\right)$ under both dry and humid conditions. The activation energy determined for the system at 0% relative humidity is about 10 kJ mol^{-1}. In the presence of moisture, the activation energy increases to around 104 kJ mol^{-1}. The increase in activation energy can reflect a transition from physisorption to chemisorption, which is expected due to the involvement of chemical bonding in the presence of moisture. In dry conditions, physisorption involves weak van der Waals forces and typically has low activation energies, often below 40 kJ mol^{-1},[69,84] and sometimes even close to zero because the process is not activated, but in humid conditions, chemisorption involves the formation of chemical bonds and is usually activated, requiring higher activation energies, often above 40 kJ mol^{-1} (Table 4).[85]

FTIR measurement

Apart from the chemisorption experiments with wet CO_2, FTIR measurements have been conducted over the surface of the polymer film, which is made of PDMAPAm$_{232}$, to investigate the change on the surface of the film before and after exposing to wet CO_2 and N_2 and results are demonstrated in Fig. 10 and 11.

Fig. 10 illustrates the FTIR spectrum of polymer PDMAPAm$_{232}$ exposed to N_2. The characteristic transmittance bands associated with specific functional groups: a methyl ($-CH_3$) deformation at 1373 cm^{-1}, C–H bending at 1461 cm^{-1}, N–H bending (amide II) at 1535 cm^{-1}, C═O stretching (amide I) at 1641 cm^{-1}, symmetric and asymmetric stretching of the dimethylamino group ($-N(CH_3)_2$) at 2765 and 2816 cm^{-1}, C–H stretching vibrations at 2857 and 2939 cm^{-1}, and a broad N–H stretching band at 3298 cm^{-1}.

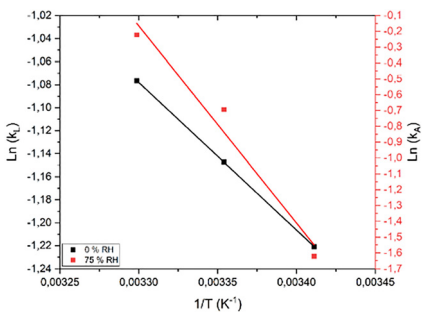

Fig. 9 Arrhenius plots for rate coefficients of Langmuir model (k_L) and Avrami model (k_A).

Table 4 Activation energies of Langmuir (k_L) and Avrami (k_A) constants

Conditions	E_a (kJ mol^{-1})
k_L of Langmuir model (dry CO_2)	10.7
k_A of Avrami model (humid CO_2)	103.6

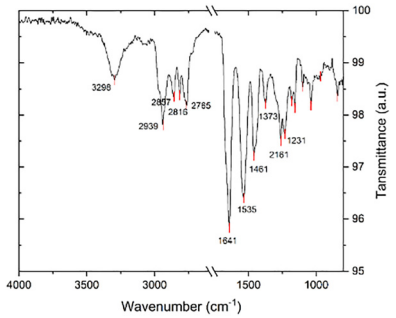

Fig. 10 FTIR spectrum of polymer PDMAPAm$_{232}$ exposed to N_2.

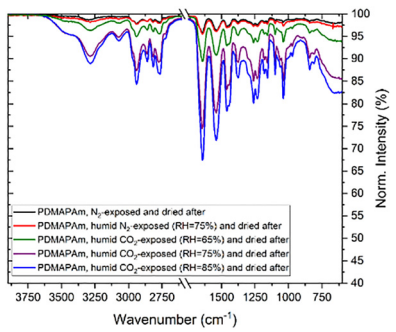

Fig. 11 FT-IR spectrum of polymer PDMAPAm$_{232}$ exposed to N_2, humid N_2 and humid CO_2 after drying them with N_2 for one night.

Fig. 11 represents FTIR spectrum of polymer PDMAPAm exposed to dry N_2, humid N_2 and humid CO_2. This is clear from the spectra that IR spectra of N_2-exposed PDMAPAm$_{232}$ serves as the baseline whereas humid N_2 shows slight intensity changes, indicating minor interactions with water. Compared to both cases, humid CO_2-exposed PDMAPAm$_{232}$ exhibits more pronounced vibration in the FTIR spectra results, suggesting stronger chemical interactions. Another important point is that as the humidity of CO_2 increases, intensity of peaks rises and especially over 75% of relative humidity, the intensity of peaks increases significantly. This is not coincidence that as shown in the Fig. 8, q_e-value (maximum uptake capacity of the polymer) also suddenly rises more than 75% of relative humidity. This may be due to formation of more bicarbonate ions at higher relative humidity conditions.[86,87]

There are two big remarkable difference between spectra of humid CO_2 and humid N_2-exposed polymer films. The first one is that the intensity of some peaks get higher when the polymer

interacts with humid CO_2 compared to humid N_2 as it was observed in another tertiary amine-based polymer.[88] The second one is that one new peak appears in the humid CO_2 case, which corresponds to (N–H) stretching vibrations from the ammonium ion (NH^+) formation,[89] arising from the formation of ammonium bicarbonate salt. The reason for both differences is the reaction that occurs between the tertiary amine of the polymer and humid CO_2, which leads to the formation of ammonium bicarbonate.[88]

Broad bands around 3300–3500 cm^{-1} are typically associated with (N–H) stretching. Symmetric and asymmetric stretching of the dimethylamino group ($-N(CH_3)_2$) appear at 2766 cm^{-1} and 2816 cm^{-1} in the N_2-exposed case, but both peaks turn out to be intense, and the peak turns out to be sharper in the humid CO_2-exposed case. This may be because they are bound to a tertiary amine that potentially reacts with humid CO_2 for the formation of (NH^+) and (HCO_3^-). The 1650–1600 cm^{-1} is a critical region for HCO_3^- asymmetric stretching. In dry N_2 and humid N_2-exposed cases, the peak at 1641 cm^{-1} corresponding to (C═O) stretching of amide is overlapping. However, the intensity of the peak increases significantly as soon as the polymer interacts with the humid CO_2. Considering that (COO–) asymmetric stretching from bicarbonate[88,90] and (C–O) asymmetric stretch of bicarbonate[59,88] appear at 1657 cm^{-1} and 1610 cm^{-1}, respectively. The reason for the higher intensity in the humid CO_2-case can be the formation of the bicarbonate.

Optimization of PDMAPAm polymer film thickness

In some other works, it is mentioned that altering the thickness of the polymeric amine film serves as a functional analogue to adjusting amine loadings within porous support material that can increase uptake capacity of material.[73,91] Therefore, three polymer solutions, 30% w/w, 10% w/w, and 2% w/w of PDMAPAm in THF were prepared and the polymer films with three different thickness were coated onto the quartz crystal as illustrated in previous publications.[40,41] Then, the CO_2 capture capacities of the polymer films were measured by changing the film thickness and are shown in Fig. 12.

Fig. 12 illustrates the amount of gas adsorbed by the polymer film when exposed to both dry and humid CO_2, as well as the portion of gas uptake attributable specifically to chemisorption, across varying film thicknesses. It can be clearly seen from Fig. 12(a) that the CO_2 uptake capacity of the polymer film increases in both dry and humid conditions as the film thickness decreases, whereas Fig. 12(b) shows the same trend for chemisorption in humid conditions. This trend fits well with the findings shown in another publication[73] described in the literature. As shown in previous publication,[40,41] the film, which was fabricated, is thick and packed. The research group of J. R. Hoffman *et al.*[73,74] has mentioned that in the thick-film regime, CO_2 capture is primarily limited by the accessibility of amine sites and amine groups located deeper within the film are often inaccessible and therefore do not effectively participate in the reaction. In other words, when the polymer thickness is higher, interaction between CO_2 and the amine group only occurs on the surface in any way. Therefore, by making the

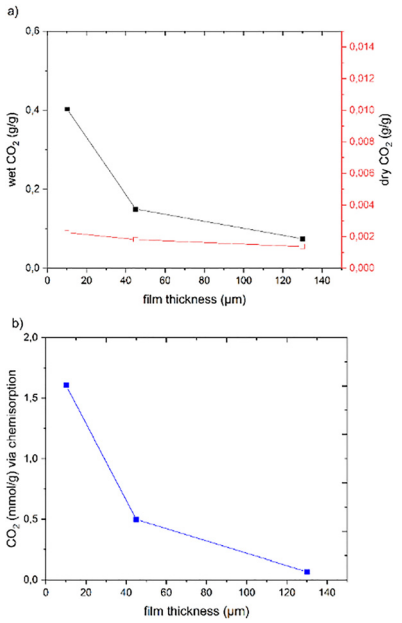

Fig. 12 (a) Overall dry and wet CO_2 uptake (physisorption + chemisorption) and (b) CO_2 chemisorption uptake changing with polymer film thickness.

polymer film thinner, the amount of polymer used for film fabrication decreases, and the surface area-to-volume ratio increases. As a result, using less polymer (thinner film), more CO_2 is captured. This is the reason why at thinner polymer films, CO_2 uptake capacity goes up in this case.

Using the impact of film thickness on the adsorption capacity, PDMAPAm and PDMAPAm-*b*-PMMA films were prepared with the smallest thickness (10 μm). CO_2 uptake capacity of the diblock copolymer was compared with the CO_2 uptake capacity of PDMAPAm polymer film. The result of comparison is demonstrated in the Fig. 13.

This is clear from Fig. 13 that generally, a homopolymer shows a higher total CO_2 uptake capacity, which is the sum of adsorbed CO_2 *via* physisorption and chemisorption, than a diblock copolymer does in humid conditions. Alone, the homopolymer adsorbs more CO_2 *via* chemisorption than the diblock copolymer, and this is due to the fact that the homopolymer has more monomeric units with a tertiary amine group than the diblock copolymer has. Most of CO_2 is adsorbed *via* physisorption by both homopolymer and diblock copolymer. However, as for physisorption, the diblock copolymer adsorbs relatively more CO_2 at dry conditions than the homopolymer does, as it has been observed for the polymers in powder form. The reason for this higher CO_2 uptake capacity of diblock copolymer at dry conditions is the existence of the PMMA group on it, as mentioned before.

Unified model

In previous work,[17] polymerization kinetics[42] were integrated with the adsorption kinetics of CO_2 on the polymer material under dry conditions, yielding a unified model. Starting from

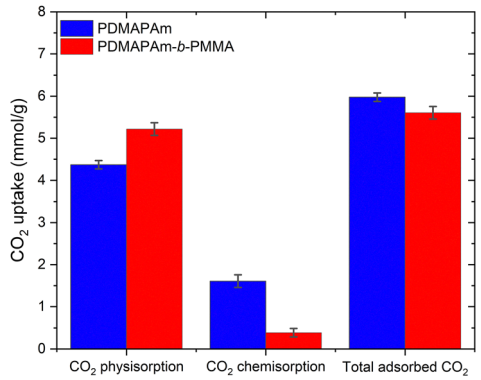

Fig. 13 CO_2 capture comparison of $PDMAPAm_{232}$ film with $PDMAPAm_{232}$-*b*-$PMMA_{57}$ film at dry and humid conditions.

molecular-level polymer design, the unified model approach establishes quantitative structure–property relationships linking polymer composition, molar mass, and block architecture to solution–diffusion-dominated CO_2 adsorption under dry conditions. The framework is subsequently extended to realistic DAC environments by explicitly incorporating humidity-dependent adsorption mechanisms, allowing simultaneous description of physisorption- and chemisorption-controlled CO_2 uptake within a single unified kinetic model. By resolving the distinct kinetic regimes, activation energies, and rate-limiting steps governing CO_2 capture in both dry and humid atmospheres, the model enables direct translation of polymer synthesis parameters and polymer properties into operational capture performance of CO_2 membrane adsorber made of the polymer. As a result, this unified methodology allows the rational design and fabrication of PDMAPAm-based polymer membrane adsorbers that achieve high CO_2 uptake capacities under dry and humid conditions, bridging the gap between polymer chemistry, adsorption science, and deployable direct air capture materials within a single coherent material-design strategy. Another important consideration is that humidity and temperature vary across different geographical locations, which implies that polymer materials can be tailored accordingly, for example by adjusting molar mass or block composition. Using the unified model, the CO_2 uptake capacity of these designed polymers can then be directly predicted under different humidity and temperature conditions without the need for extensive experimental screening, thereby significantly reducing time and experimental effort.

The unified model could predict polymer properties of the synthesized polymer PDMAPAm and the CO_2 uptake of it correctly in dry conditions. In this study, the kinetic model for CO_2 adsorption under humid conditions was developed and integrated into a unified framework to support digital-twin-assisted design of CO_2-responsive polymers. For consistency and comparative analysis, the same polymer, $PDMAPAm_{163}$, used in our previous work was selected as the case study material (SI).

The humid CO_2 adsorption isotherm of the polymer, PDMAPAm, was also simulated using the prediction line (Fig. 8), which describes how the kinetic parameters (q_e and k_A) change with relative humidity. To test whether the Avrami model predicts correctly, humid CO_2 adsorption isotherms of the homopolymer were experimentally measured and compared with the simulation shown in Fig. 14.

It can be clearly seen from Fig. 14 that the humid CO_2 adsorption model accurately predicted the polymer's uptake capacity, indicating that the model performs reliably under these conditions. With this, the unified model can simulate an optimal recipe of polymer synthesis and its properties and at the same time CO_2 uptake capacity of the polymer in dry and humid conditions.

The resulting unified model therefore functions as a materials design tool that can be universally applied to design CO_2-responsive polymers, starting from the design of a monomer that also enables to predict optimal polymer synthesis recipe, polymerization time, polymer properties and CO_2-capture process conditions for the polymers of interest and can also optimize CO_2 uptake capacity of developed polymers as a function of polymer properties and CO_2 capture process conditions.

Comparison of CO_2 uptake capacity of PDMAPAm and PDMAPAm-*b*-PMMA with polymer-based adsorbents

The adsorption performance of the developed polymer materials for CO_2 capture was assessed under identical conditions (25 °C, 1 bar) in both dry and humid environments. The Table 5 compares CO_2 uptake capacity of $PDMAPAm_{232}$ and $PDMAPAm_{232}$-*b*-$PMMA_{57}$ with other polymer-based adsorbers under different conditions.

Under dry conditions (25 °C, 1 bar), $PDMAPAm_{232}$ exhibited a modest uptake of 0.05 mmol g^{-1}, while its block copolymer $PDMAPAm_{232}$-*b*-$PMMA_{57}$ achieved a significantly higher uptake of 0.52 mmol g^{-1}. In comparison, polyethyleneimine (PEI)—a benchmark polymer for CO_2 adsorption—shows a dry uptake of 2.10 mmol g^{-1}, outperforming both polymers from this study.

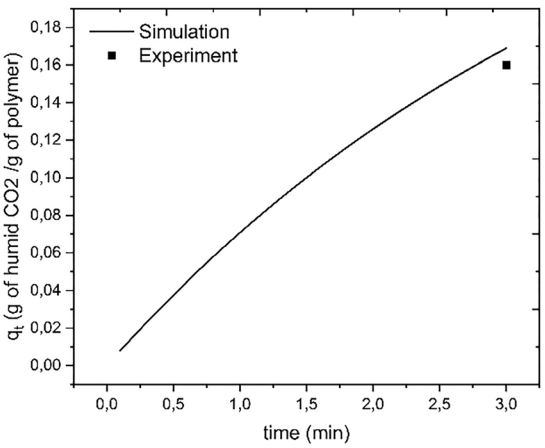

Fig. 14 A comparison between the kinetic model predictions and experimental data for CO_2 adsorption under humid conditions on the PDMAPAm163 homopolymer is presented. The measurements were conducted at room temperature, atmospheric pressure, and a relative humidity of 80%.

Table 5 Comparison of CO_2 uptake capacity of PDMAPAm and PDMAPAm-*b*-PMMA with other polymer-based adsorbers

Polymer-based adsorbents	CO_2 uptake capacity (mmol g^{-1})	Conditions	Ref.
$PDMAPAm_{232}$	0.05	25 °C, 1 bar, dry CO_2	This study
$PDMAPAm_{232}$-*b*-$PMMA_{57}$	0.52	25 °C, 1 bar, dry CO_2	This study
$PDMAPAm_{232}$-*b*-$PMMA_{57}$	5.60	25 °C, 1 bar, humid CO_2, RH = 75%	This study
$PDMAPAm_{232}$	6.00	25 °C, 1 bar, humid CO_2, RH = 75%	This study
SBA-15-supported linear PEI	0.20–0.80	25 °C, 1 bar, dry CO_2	92–94
SBA-15-supported branched PEI	0.50–1.50	25 °C, 1 bar, dry CO_2	95–97
SBA-15-supported branched PEI	1.70–2.00	25 °C, 1 bar, humid CO_2, RH = 50%	95–97
Al_2O_3-supported branched PEI	1.70–1.80	25 °C, 1 bar, dry CO_2	94 and 98
Quaternized chitosan/poly(vinyl alcohol)	0.20	25 °C, 1 bar, dry CO_2	94
Tetraethylenepentamine (TEPA) "ZS-T-60"	1.00–1.10	25 °C, 1 bar, dry CO_2	99
SiO_2-supported tetraethylenepentamine (TEPA)	1.00–2.50	25 °C, 1 bar, dry CO_2	100
Polyacrylonitrile (PAN)	0.40	25 °C, 1 bar, dry CO_2	101
PAN-PEI	0.20		
PAN-DETA	1.80		
MIL-101(Cr)-supported-polypropylenimine (PPI)	1.20–1.30	25 °C, 1 bar, dry CO_2	93,94
MIL-101(Cr)-supported-polypropylenimine (PPI)	1.30–1.60	25 °C, 1 bar, humid CO_2, RH = 50%	102
Lewatit® VP OC 1065	2.00–2.50	25 °C, 1 bar, humid CO_2, RH = 40–80%	103

Another point: SBA-15-supported linear PEI ranges from 0.20–0.80 mmol g^{-1}, while branched PEI supported on SBA-15 ranges from 0.50–1.50 mmol g^{-1}, indicating that structural optimization and support materials play critical roles. Other polymers, such as quaternized chitosan/poly(vinyl alcohol) and polyacrylonitrile (PAN) show lower uptakes of 0.20 mmol g^{-1} and 0.40 mmol g^{-1}, respectively, under dry conditions. tetraethylenepentamine (TEPA) supported on silica (SiO_2) performs better, with uptakes ranging from 1.00–2.50 mmol g^{-1}, depending on the support and formulation.

Under humid conditions, conventional polymer sorbents based on amine-functionalized polyacrylonitrile (PAN), and tetraethylenepentamine (TEPA), including PAN-DETA, PAN-PEI, and PAN-TEPA, exhibit relatively low CO_2 uptake capacities (typically $\leq$2 mmol g^{-1}).[99–101] Similarly, polymer–amine composites relying on the impregnation of low-molecular-weight amines or branched PEI onto polymeric or inorganic supports and Lewatit generally achieve moderate CO_2 uptake capacities in the range of 2–3 mmol g^{-1}.[94–98] In comparison, the $PDMAPAm_{232}$ membrane adsorber demonstrates a markedly higher CO_2 uptake of approximately 6 mmol g^{-1}, surpassing most reported polymer-based sorbents and underscoring the effectiveness of densely distributed tertiary amine groups within a thin, continuous polymer film. The diblock copolymer $PDMAPAm_{232}$-*b*-$PMMA_{57}$ maintains a comparably high CO_2 uptake capacity, with only a modest decrease relative to the $PDMAPAm_{232}$, demonstrating that incorporation of a PMMA block improves mechanical robustness without severely compromising adsorption performance.[38–40]

Overall, the comparison demonstrates that both PDMAPAm and PDMAPAm-*b*-PMMA outperform a wide range of commercial polymer-based CO_2 sorbents, showing the new developed polymers as promising candidates for fabrication of CO_2 membrane adsorbers to implement direct air capture technology.

Conclusion

This study provides a comprehensive investigation into the CO_2 capture behavior of the CO_2-responsive homopolymer PDMAPAm and its diblock copolymer PDMAPAm-*b*-PMMA for fabrication of CO_2 membrane adsorbers, with a focus on their applicability as membrane adsorbers for direct air capture (DAC) technologies. Through a systematic approach, the adsorption mechanisms were delineated into physisorption and chemisorption processes, depending on the moisture content of the CO_2 stream and investigated.

As mentioned in previous publication,[17] under dry conditions, CO_2 was found to undergo physisorption, interacting primarily with the tertiary amine groups of PDMAPAm and the carbonyl functionalities of PMMA. In contrast, in humid CO_2, chemisorption also occurs through bicarbonate formation at the tertiary amine sites, as confirmed by mass changes, calorimetry, and characteristic FTIR bands. Nevertheless, physisorption remains the dominant uptake pathway under humid conditions, with the physically adsorbed fraction exceeding the chemisorbed fraction by several-fold.

Beyond mechanistic characterization, the study explored the kinetics of CO_2 adsorption, incorporating both physisorption and chemisorption kinetics into the kinetics of polymer synthesis in a unified model for digital-twin supported design of CO_2-responsive polymers. The primary novelty of this work is the development of a unified kinetic model that, for the first time, integrates polymerization kinetics with adsorption kinetics, enabling direct prediction of CO_2 uptake capacity from the intrinsic polymer properties. A second key innovation is the application of this model to rationally design and fabricate a membrane adsorber that achieves a CO_2 uptake capacity of 6 mmol g^{-1} significantly surpassing the performance of commercially available polymer-based sorbents. The results highlight the strong potential of PDMAPAm-based materials in addressing the pressing need for effective DAC solutions, contributing meaningfully to the broader scientific effort to mitigate atmospheric CO_2 levels through innovative material development.

Conflicts of interest

There are no conflicts to declare.

Data availability

All data supporting this study are provided in the supplementary information (SI) and previous published dataset. Supplementary information: synthesis procedure, structural characterization, theoretical calculations, experimental methods, and spectral analyses. See DOI: https://doi.org/10.1039/d6mh00641h.

For access to the dataset, refer to DOI: https://doi.org/10.5281/zenodo.17963415.

Acknowledgements

The authors are grateful for financial support from Direct Air Capture and Storage (DACStorE) (KA2-HSC-12) offered by the Initiative and Networking Fund of the Helmholtz Association. Additionally, the authors thank Silvio Neumann and Maren Brinkmann for performing the NMR and GPC measurements as well as Dr. Felix Kandelhard for discussion on the polymerization kinetics. Scientific discussions with Prof. Dr. Volker Abetz are greatly acknowledged.

References

1 M. Erans, E. S. Sanz-Pérez, D. P. Hanak, Z. Clulow, D. M. Reiner and G. A. Mutch, *Energy Environ. Sci.*, 2022, **15**, 1360–1405.
2 X. Zhu, W. Xie, J. Wu, Y. Miao, C. Xiang, C. Chen, B. Ge, Z. Gan, F. Yang and M. Zhang, *Chem. Soc. Rev.*, 2022, **51**, 6574–6651.
3 L. Küng, S. Aeschlimann, C. Charalambous, F. McIlwaine, J. Young, N. Shannon, K. Strassel, C. N. Maesano, R. Kahsar and D. Pike, *Energy Environ. Sci.*, 2023, **16**, 4280–4304.
4 J. Kotowicz, K. Niesporek and O. Baszczeńska, *Energies*, 2025, **18**, 496.
5 P. Webb, H. Muslemani, M. Fulton and N. Curson, *Scaling Direct Air Capture (DAC): A moonshot or the sky's the limit?*, OIES Paper: CM, 2023.
6 Y. Zhang, J. Feng, L. Li, S. Zhao, C. Wu, Z. Huang and H. Lin, *Front. Energy*, 2025, 1–13.
7 D. Panda, V. Kulkarni and S. K. Singh, *React. Chem. Eng.*, 2023, **8**, 10–40.
8 J. Young, F. Mcilwaine, B. Smit, S. Garcia and M. Van der Spek, *Chem. Eng. J.*, 2023, **456**, 141035.
9 U. I. Premadasa, N. Kumar, D. Stamberga, V. Bocharova, J. T. Damron, T. Li, S. Roy, Y.-Z. Ma, V. S. Bryantsev and B. Doughty, *J. Chem. Phys.*, 2024, **161**, 164707.
10 J. Serafin and B. Dziejarski, *Microporous Mesoporous Mater.*, 2023, **354**, 112513.
11 C. Erkey, in *Supercritical fluid science and technology*, Elsevier, 2011, vol. 1, pp. 41–77.
12 J. C. Pashin, in *Applied coal petrology*, Elsevier, 2008, pp. 227–262.
13 D. A. Bell, B. F. Towler and M. Fan, *Coal gasification and its applications*, William Andrew, 2010.
14 I. Sarbu and I. Sarbu, *Solar heating and cooling systems*, Springer, 2021.
15 C. Tien, *Introduction to adsorption: Basics, analysis, and applications*, Elsevier, 2018.
16 D. Webb, P. Rowston and G. McNeill, *ASEG Extended Abstracts*, 2003, **2003**, 1–4.
17 E. Pashayev and P. Georgopanos, *J. Mater. Chem. A*, 2026, **14**, 15735.
18 M. Soukri, P. Sitaula, D. O'Nolan, M. G. Izenson and S. D. Phillips, *Development of Advanced Solid Sorbents for Direct Air Capture*, RTI International, Research Triangle Park, NC (United States), 2023.
19 L. B. Hamdy, C. Goel, J. A. Rudd, A. R. Barron and E. Andreoli, *Mater. Adv.*, 2021, **2**, 5843–5880.
20 R. B. Said, J. M. Kolle, K. Essalah, B. Tangour and A. Sayari, *ACS Omega*, 2020, **5**, 26125–26133.
21 C. Zhang, J. Zhou, X. Ye, Z. Li and Y. Wang, *J. Membr. Sci.*, 2022, **641**, 119928.
22 M.-S. Lebrun-Chopra, The Development of Novel Bio-Based CO_2-Responsive Polymers for Binder Applications, PhD thesis, Queen's University (Canada), 2021.
23 Y.-T. Shieh, Y.-T. Lin and C.-C. Cheng, *Carbohydr. Polym.*, 2017, **170**, 281–288.
24 K. Bauri, A. Pan, U. Haldar, A. Narayanan and P. De, *J. Polym. Sci., Part A: Polym. Chem.*, 2016, **54**, 2794–2803.
25 A. Riabtseva, S. N. Ellis, P. Champagne, P. G. Jessop and M. F. Cunningham, *Ind. Eng. Chem. Res.*, 2021, **60**, 9807–9816.
26 M. F. Cunningham and P. G. Jessop, *Macromol. React. Eng.*, 2022, **16**, 2200031.
27 M. F. Cunningham and P. G. Jessop, *Chem. Commun.*, 2023, **59**, 13272–13288.
28 M. F. Cunningham and P. G. Jessop, *Eur. Polym. J.*, 2016, **76**, 208–215.
29 W. Ji, D. Panus, R. N. Palumbo, R. Tang and C. Wang, *Biomacromolecules*, 2011, **12**, 4373–4385.
30 S. Demirci, S. D. Sutekin, O. Guven and N. Sahiner, *Int. J. Hydrogen Energy*, 2023, **48**, 23002–23012.
31 E. Pashayev, F. Kandelhard and P. Georgopanos, *Macromol. React. Eng.*, 2023, **17**, 2200068.
32 R. Du, A. Chakma and X. Feng, *J. Membr. Sci.*, 2007, **290**, 19–28.
33 Z. Zhou, T. Liu, A. U. Khan and G. Liu, *Sci. Adv.*, 2019, **5**, eaau6852.
34 A. Esmeraldo Paiva, J. F. Baez Vasquez, A. Selkirk, N. Prochukhan, F. G. L. Medeiros Borsagli and M. Morris, *ACS Appl. Mater. Interfaces*, 2022, **14**, 35265–35275.
35 K. Nieswandt, P. Georgopanos and V. Abetz, *Polym. Chem.*, 2021, **12**, 2210–2221.
36 R. Shevate, M. Kumar, M. Karunakaran, C. Canlas and K.-V. Peinemann, *J. Mater. Chem. A*, 2018, **6**, 4337–4345.
37 L. Tsaur and U. B. Wiesner, *Polymers*, 2023, **15**, 2020.
38 F. Kandelhard, K. Schuldt, J. Schymura, P. Georgopanos and V. Abetz, *Macromol. React. Eng.*, 2021, **15**, 2000058.
39 F. Kandelhard, E. Pashayev, J. Schymura and P. Georgopanos, *Ind. Eng. Chem. Res.*, 2023, **62**, 8696–8708.

40 E. Pashayev and P. Georgopanos, *Macromol. Mater. Eng.*, 2025, **310**, 2400290.
41 E. Pashayev and P. Georgopanos, *Chem. Ing. Tech.*, 2025, **97**, 703–709.
42 E. Pashayev and P. Georgopanos, *Polymers*, 2025, **17**, 1115.
43 G. Desmet, N. Rybel and P. Steenberge, *Macromol. Rapid Commun.*, 2017, **39**, 1700403.
44 F. Sandra, N. Klein, M. Leistner, M. R. Lohe, M. Benusch, M. Woellner, J. Grothe and S. Kaskel, *Ind. Eng. Chem. Res.*, 2015, **54**, 6677–6682.
45 A. Werner, M. Wöllner, P. Bludovsky, M. Leistner, C. Selzer and S. Kaskel, *Microporous Mesoporous Mater.*, 2018, **268**, 46–49.
46 M. Wöllner, N. Klein and S. Kaskel, *Microporous Mesoporous Mater.*, 2019, **278**, 206–211.
47 C. Lu and A. W. Czanderna, *Applications of piezoelectric quartz crystal microbalances*, Elsevier, 2012.
48 G. Sauerbrey, *Z. Phys.*, 1959, **155**, 206–222.
49 Y. G. Ko, S. S. Shin and U. S. Choi, *J. Colloid Interface Sci.*, 2011, **361**, 594–602.
50 P. Bollini, S. A. Didas and C. W. Jones, *J. Mater. Chem.*, 2011, **21**, 15100–15120.
51 E. Orestes, C. M. Ronconi and J. W. de Mesquita Carneiro, *Phys. Chem. Chem. Phys.*, 2014, **16**, 17213–17219.
52 M. Haris, A. Aziz, M. Sohail and W. Sardar, *Environ. Sci. Pollut. Res.*, 2025, 1–19.
53 J. F. Liebman and A. Greenberg, *Struct. Chem.*, 2019, **30**, 1631–1634.
54 J. DeRuiter, *Princ. Drug Action*, 2005, **1**, 1–16.
55 G. L. Beutner, I. S. Young, M. L. Davies, M. R. Hickey, H. Park, J. M. Stevens and Q. Ye, *Org. Lett.*, 2018, **20**, 4218–4222.
56 F. S. Parker and F. S. Parker, *Applications of infrared spectroscopy in biochemistry, biology, and medicine*, 1971, pp. 165–172.
57 T. L. Donaldson and Y. N. Nguyen, *Ind. Eng. Chem. Fundam.*, 1980, **19**, 260–266.
58 P. D. Vaidya and E. Y. Kenig, *Ind. Eng. Chem. Res.*, 2008, **47**, 34–38.
59 J. J. Lee, C.-H. Chen, D. Shimon, S. E. Hayes, C. Sievers and C. W. Jones, *J. Phys. Chem. C*, 2017, **121**, 23480–23487.
60 A. A. Al-Absi, M. Mohamedali, A. Domin, A. M. Benneker and N. Mahinpey, *Chem. Eng. J.*, 2022, **447**, 137465.
61 W. R. Lee, H. Jo, L.-M. Yang, H. Lee, D. W. Ryu, K. S. Lim, J. H. Song, D. Y. Min, S. S. Han and J. G. Seo, *Chem. Sci.*, 2015, **6**, 3697–3705.
62 M. Lotfinezhad, M. Tahmasebpoor and C. Pevida, *Environ. Sci. Pollut. Res.*, 2024, 1–14.
63 R. Navik, E. Wang, X. Ding, K. Qiu and J. Li, *Environ. Chem. Lett.*, 2024, **22**, 1791–1830.
64 M. Zhao, L. Huang, Y. Gao, Z. Wang, S. Liang, X. Zhu, Q. Wang, H. He and D. O'Hare, *Nano-Micro Lett.*, 2025, **17**, 1–19.
65 P. Singh, J. P. Niederer and G. F. Versteeg, *Chem. Eng. Res. Des.*, 2009, **87**, 135–144.
66 X. Deng, Y. Han, L.-C. Lin and W. W. Ho, *Sep. Purif. Technol.*, 2022, **299**, 121601.
67 A. Maiti, W. Bourcier and R. Aines, *CO_2* capture in primary and tertiary amines-insights from atomistic modeling, Lawrence Livermore National Lab.(LLNL), Livermore, CA (United States), 2010.
68 Q. Grossmann, P. A. Saenz-Cavazos, N. Ferru, D. R. Williams and M. Mazzotti, *Ind. Eng. Chem. Res.*, 2025, **64**, 7165–7175.
69 H. J. Kreuzer and Z. W. Gortel, *Physisorption kinetics*, Springer Science & Business Media, 2012.
70 O. D. Agboola and N. U. Benson, *Front. Environ. Sci.*, 2021, **9**, 678574.
71 F. Huber, J. Berwanger, S. Polesya, S. Mankovsky, H. Ebert and F. J. Giessibl, *Science*, 2019, **366**, 235–238.
72 W. Ranke, *Adsorption and desorption*, Fritz-Haber-Institut der Max-Planck-Gesellschaft, Berlin, 2008.
73 J. R. Hoffman, A. E. Baumann and C. M. Stafford, *Chem. Eng. J.*, 2025, **507**, 160347.
74 J. R. Hoffman, A. E. Baumann and C. M. Stafford, *Chem. Eng. J.*, 2024, **481**, 148381.
75 M. E. Potter, K. M. Cho, J. J. Lee and C. W. Jones, *ChemSusChem*, 2017, **10**, 2192–2201.
76 Q. Grossmann, V. Stampi-Bombelli, A. Yakimov, S. Docherty, C. Copéret and M. Mazzotti, *Ind. Eng. Chem. Res.*, 2023, **62**, 13594–13611.
77 S. M. Lalji, M. Ayubi, S. I. Ali, S. U. Rahman and M. Mustafa, *Discover Chem.*, 2024, **1**, 71.
78 K. Pirzadeh, A. A. Ghoreyshi, S. Rohani and M. Rahimnejad, *Ind. Eng. Chem. Res.*, 2019, **59**, 366–378.
79 G. Blanchard, M. Maunaye and G. Martin, *Water Res.*, 1984, **18**, 1501–1507.
80 N. Álvarez-Gutiérrez, M. Gil, F. Rubiera and C. Pevida, *Chem. Eng. J.*, 2017, **307**, 249–257.
81 R. Serna-Guerrero and A. Sayari, *Chem. Eng. J.*, 2010, **161**, 182–190.
82 S. S. Fatima, A. Borhan, M. Ayoub and N. A. Ghani, *Processes*, 2023, **11**, 2833.
83 T. A. Saleh and A. A. Al-Absi, *J. Mol. Liq.*, 2017, **248**, 577–585.
84 M. B. Yahia and S. Wjihi, *Sci. Rep.*, 2020, **10**, 16118.
85 T. J. Wolery, *Geochemistry*, Springer, 1998, pp. 5–6.
86 É. C. Lima, M. A. Adebayo and F. M. Machado, *Carbon nanomaterials as adsorbents for environmental and biological applications*, Springer, 2015, pp. 33–69.
87 G. A. Russell-Parks, N. Leick, M. A. Marple, N. A. Strange, B. G. Trewyn, S. H. Pang and W. A. Braunecker, *J. Phys. Chem. C*, 2023, **127**, 15363–15374.
88 H. Xu, S. G. Pate and C. P. O'Brien, *J. Membr. Sci.*, 2024, **689**, 122163.
89 S. Petit, D. Righi and J. Madejová, *Appl. Clay Sci.*, 2006, **34**, 22–30.
90 G. S. Foo, J. J. Lee, C. H. Chen, S. E. Hayes, C. Sievers and C. W. Jones, *ChemSusChem*, 2017, **10**, 266–276.
91 J. Yu, Y. Zhai and S. S. Chuang, *Ind. Eng. Chem. Res.*, 2018, **57**, 4052–4062.
92 N. Gargiulo, A. Peluso, P. Aprea, F. Pepe and D. Caputo, *J. Chem. Eng. Data*, 2014, **59**, 896–902.

93 S. H. Pang, R. P. Lively and C. W. Jones, *ChemSusChem*, 2018, **11**, 2628–2637.
94 M. Robertson, J. Qian and Z. Qiang, *ACS Appl. Polym. Mater.*, 2024, **6**, 14169–14189.
95 A. Holewinski, M. A. Sakwa-Novak and C. W. Jones, *J. Am. Chem. Soc.*, 2015, **137**, 11749–11759.
96 W. Chaikittisilp, H.-J. Kim and C. W. Jones, *Energy Fuels*, 2011, **25**, 5528–5537.
97 A. Holewinski, M. A. Sakwa-Novak, J.-M. Y. Carrillo, M. E. Potter, N. Ellebracht, G. Rother, B. G. Sumpter and C. W. Jones, *J. Phys. Chem. B*, 2017, **121**, 6721–6731.
98 M. A. Sakwa-Novak and C. W. Jones, *ACS Appl. Mater. Interfaces*, 2014, **6**, 9245–9255.
99 Y. Jia, J. Wei, Y. Yuan, L. Geng, S. Chen and L. Liao, *J. Mater. Res.*, 2022, **37**, 543–553.
100 Z. Yang, Y. Zhou, H. Cui, Z. Cheng and Z. Zhou, *Front. Chem. Sci. Eng.*, 2025, **19**, 9.
101 Y. Kuang, H. He, S. Chen, J. Wu and F. Liu, *Adsorption*, 2019, **25**, 693–701.
102 R. A. Yang, S. Cho, S. N. Hughes and M. L. Sarazen, *ChemSusChem*, 2024, **17**, e202400249.
103 M.-Y. A. Low, D. Danaci, H. Azzan, R. T. Woodward and C. Petit, *J. Chem. Eng. Data*, 2023, **68**, 3499–3511.

